Tuning the magnetic and electronic properties of bilayer graphene nanoribbons on Si(001) by bias voltage

Zhuhua Zhang,[1,2] Changfeng Chen,[3] Xiao Cheng Zeng,[2] and Wanlin Guo[1,*]
[1]*Institute of Nanoscience, Nanjing University of Aeronautics and Astronautics, Nanjing 210016, China*
[2]*Department of Chemistry, University of Nebraska–Lincoln, Lincoln, Nebraska 68588, USA*
[3]*Department of Physics and High Pressure Science and Engineering Center, University of Nevada, Las Vegas, Nevada 89154, USA*
(Received 4 December 2009; revised manuscript received 28 February 2010; published 13 April 2010)

We report on a systematic study of bias-voltage-induced modulation of magnetic and electronic properties of bilayer zigzag graphene nanoribbons (Z-GNRs) on Si(001) substrate by first-principles calculations. We show that the intrinsically nonmagnetic bilayer Z-GNRs exhibit magnetic ordering on the top layer while the bottom layer serves as a nonmagnetic buffer layer when adsorbed on the substrate. Interestingly, the adsorbed bilayers display distinct ribbon-width-dependent magnetoelectric effect under bias voltages. The magnetoelectric coefficient oscillates with increasing ribbon width, which arises from an interesting interplay of the interaction of the bottom ribbon layer with the substrates and the decay length of the localized edge states in Z-GNRs. Moreover, our calculations reveal that the electronic band gap of the top ribbon layer also can be effectively modulated by the applied bias voltage, which can lead to a semiconductor-to-metal transition in the top magnetic semiconductor layer. These results provide insights into the intriguing behaviors of Z-GNRs on substrates and raise the prospects of developing an innovative path toward graphene-based electronic and spintronic devices by integrating the emerging nanoscale graphene systems with existing silicon technology.

DOI: 10.1103/PhysRevB.81.155428 PACS number(s): 73.22.−f, 75.70.Ak, 73.20.−r, 71.15.Mb

I. INTRODUCTION

Control of magnetization by electric fields is ideally suited for nanoelectronic and spintronic devices since it offers the best of the two realms: crucial functionalities and device concepts compatible with existing technology.[1] The magnetoelectric (ME) effect,[2,3] which determines the induction of magnetization by an electric field and or induction of polarization by means of a magnetic field, provides a promising route to serve this purpose. In particular, linear ME effect has long been pursued for practical applications since it allows a linear interplay between the induced magnetization M and external electric field E, $\mu_0 M_i = \alpha_{ij} E_j$, where α_{ij} is the linear ME coefficients and μ_0 the permeability of free space.[4] This fundamental physical effect was first proposed[5] for chromium sesquioxide and soon observed[6] experimentally in 1960. However, the ME effect in traditional ME materials was not strong enough to attract wide attention for possible practical applications in the subsequent 40 years. In the meantime, two mechanisms for the ME effect were established substantially. First, in conventional single-phase ME materials, field-induced displacement of ions modifies the magnetic exchange interactions, leading to changes in the system magnetization.[5] Second, in composite multiferroic materials, the ME coupling is an interface coupling effect, that is, electric field-induced strain in ferroelectric component is transferred to the ferromagnetic component to induce changes in magnetization.[7] In recent years, rapid developments in experimental techniques for the production and growth of multiferroics have fuelled a renaissance of research interest in magnetoelectrics.[8–10] Electrically controlled ferromagnetism with sizable ME coefficient has been experimentally realized in various multiferroic films and composites.[11–15] Improved quantum-mechanics-based computational techniques and capability also enable further developments of different ME coupling mechanisms. Recent theoretical studies have predicted linear ME coupling in dielectric/ferromagnet multilayer heterostructures[2,16] and ferromagnetic metal films.[17] The predicted ME effect originates from an entirely different mechanism that roots in spin-dependent screening of the electric field, which occurs between two adjacent insulator/ferromagnet interfaces so that the induced interface magnetization varies linearly with the applied field. Although the ME materials being discovered and designed are diverse, all the proposed ME mechanisms mentioned above are restricted to transition metals or metal-related materials, where localized d orbitals are crucial to the coupling between the ferroelectric and magnetic orderings.

We recently explored the ME coupling in zigzag graphene nanoribbons (Z-GNRs) on silicon substrates and demonstrated that significant ME effect can also occur in these nonmetallic systems that contain only sp electrons.[18] Strong linear ME coupling in Z-GNRs is attributed to the bias-voltage-induced charge transfer between the GNR and substrate which controls the exchange splitting of the localized edge states in the GNR. While that work has established the atomistic mechanism and main physical pictures for this phenomenon, several fundamental questions regarding the magnetic and electronic properties of the ME systems remain to be explored by more comprehensive investigations: (1) a single-layer Z-GNR shows ferromagnetic coupling of spins along the ribbon edges and antiferromagnetical coupling between the two magnetic edges but a freestanding bilayer Z-GNR has been predicted to be nonmagnetic.[19,20] It is natural to ask why the magnetic ordering reappears in the bilayer Z-GNRs adsorbed on the substrate and how the magnetization distribution changes with the bias voltage. (2) The Z-GNRs have shown distinct width effect with their electronic, magnetic, and optical properties.[21–23] In particular, when single-layer Z-GNRs are adsorbed on silicon sub-

strates, they possess semiconducting or metallic character depending on the ribbon width.[24] So, how the ME effect in the adsorbed bilayer Z-GNR changes with ribbon width also deserves further study. (3) The magnetic properties are actually determined by the electronic structures of the host materials and the magnetic modulation actually implies the change in electronic properties. Previous experimental studies have shown that applied electric field can considerably change the electron density at the Fermi level in ordered iron-platinum and iron-palladium intermetallic compounds, thereby modifying the number of unpaired *d* electrons and the magnetocrystalline anisotropy.[14] Theoretical studies have also revealed that the semiconducting Z-GNRs can be converted into half metals by applying an in-plane external electric field,[25] accompanied by change in their edge magnetization. As such, what is the relation between the applied bias voltage and the electronic properties in the adsorbed bilayer GNR systems?

In this paper, we report on a comprehensive study of the electronic and magnetic properties of bilayer Z-GNRs on Si(001) substrate under bias voltages by using first-principles calculations. The adsorbed bilayer Z-GNR shows spontaneous magnetic ordering concentrated on the top GNR layer while the bottom layer acts as a buffer layer due to the decreased interlayer interaction. The bias voltage can modulate the magnitude of the edge magnetization but does not change the character of the spin orderings. The calculated ME coefficient oscillates with increasing ribbon width and is expected to converge in wider Z-GNRs. The width-dependent oscillation is ascribed to the combined effect of the interaction of the bottom GNR layer with the substrate and the inherent width effect of the localized edge states in Z-GNRs. Concomitant with the ME coupling, the band gap of the top-layer Z-GNR is also significantly modulated by the applied bias voltage, leading to a semiconductor-to-metal transition under bias voltages beyond a critical value due to the field-induced doping effect. These results raise the prospect of future field-effect electric switch and tunable magnetic devices based on Z-GNRs integrated with silicon substrates.

II. MODELS AND METHODS

The first-principles calculations are performed within the framework of density-functional theory as implemented in the Vienna *ab initio* simulation package code.[26,27] Ultrasoft pseudopotentials for the core region and local spin-density approximation for the exchange-correlation potential are employed. A kinetic energy cutoff of 530 eV is used in the plane-wave expansion. The structural models contain bilayer Z-GNRs in AB stacking on the Si(001) substrate consisting of seven silicon monolayers in a 2×6 surface unit cell. We also performed test calculations using a larger 2×8 surface slab and obtained quantitatively the same results as those with the 2×6 surface unit cell. The dangling bonds of silicon atoms of the bottom layer and carbon atoms at the GNR edges are uniformly terminated by hydrogen atoms. The positions of silicon atoms of the topmost six monolayers plus the entire GNR atoms under each applied bias voltage are relaxed by conjugate gradient method until the force on each atom is less than 0.02 eV/Å, which is sufficient for the convergence of edge magnetization in GNRs. We set up a vacuum region of 12.5 Å to avoid the interaction between two adjacent images. The two-dimensional Brillouin-zone integration is sampled by up to 12 special *k* points for structural optimization and 24 *k* points for electronic-structure calculations. Three primitive unit cells of Z-GNRs are chosen to match the double silicon surface unit cell, with the GNRs initially stretched by about 3%. The external electric field is introduced by planar dipole-layer method.[28]

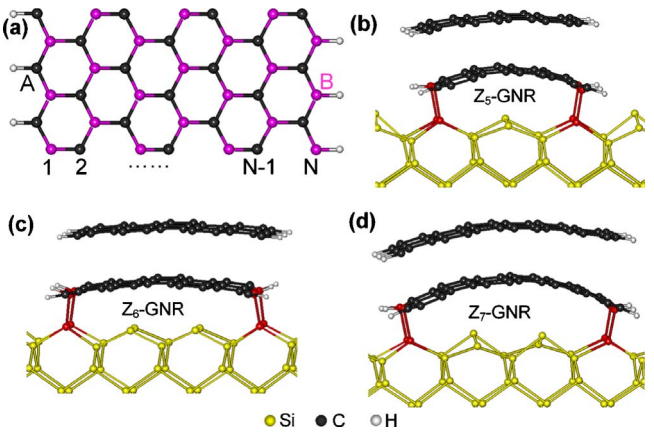

FIG. 1. (Color online) Most favorable adsorption configurations for bilayer Z-GNRs on Si(001) substrate. (a) Schematic illustration of a Z_N-GNR (N=7 in this example). [(b)–(d)] Front views of the adsorbed configurations for bilayer Z-GNRs on the Si(001) substrate.

III. RESULTS AND DISCUSSIONS

A. Structural and electronic properties for bilayer Z-GNRs on Si(001) without bias voltage

We denote the Z-GNR containing N zigzag atomic chains (N) across the ribbon width as Z_N-GNR following established convention, as shown in Fig. 1(a). To search all possible adsorption positions, the bilayer Z-GNR is moved on the silicon surface by 5 Å per step along the directions parallel and perpendicular to the Si dimer rows, respectively, and at each step the system is optimized. We compare the binding energies of all the optimized structures to determine the most energetically favorable adsorption configurations. The most stable configurations for the bilayer Z_5-, Z_6-, and Z_7-GNRs adsorbed on the substrate are shown in Figs. 1(b)–1(d). In these configurations, the GNR bilayers are adsorbed perpendicular to the Si dimer rows, with four covalent Si-C bonds symmetrically located at both ribbon edges of the bottom layer. The edge preference at the bottom layer to form covalent bonds during adsorption is due to the active edge states that are dominantly localized on the edge carbon atoms. We also obtain metastable adsorption sites when the Z-GNRs are parallel to the Si dimer rows, where the Si-C bonds are also located at the ribbon edges. All the adsorption features are consistent with the case of single-layer Z-GNRs on the same substrate.[24] The top GNR layer is weakly bound to the underlying layer at an average interlayer distance

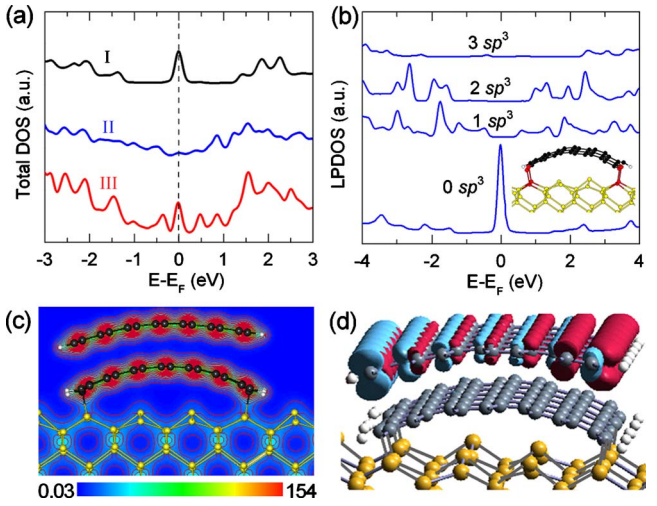

FIG. 2. (Color online) Total spin-unpolarized electron DOS of the (i) freestanding Z_7-GNR, (ii) the bottom, and (iii) top layers in the adsorbed bilayer Z_7-GNR. (b) Variation in local partial DOS of the $2p$ states of a sp^2 edge carbon atom in adsorbed single-layer Z_7-GNR with the number of sp^3 bonds in a ribbon edge. The sp^3 bonds at two ribbon edges are set symmetrically. The configuration for the case of 0 sp^3 bond is illustrated. (c) Total charge density of the bilayer Z_7-GNR adsorbed on Si(001). (d) Isosurface plots (0.15 e/Å^3) of spin density of absorbed bilayer Z_7-GNR on the Si substrate, where the magnetization density with opposite directions are marked in two different colors.

around 3.38 Å, slightly larger than the bulk graphite value of 3.35 Å, and curved to the same shape as the bridgelike bottom layer for all the studied bilayer Z-GNRs. The weak coupling from the bottom layer is also supported by the total charge-density distribution in the adsorbed Z_7-GNR bilayer system shown in Fig. 2(c), where the overlap of charge density in the interlayer spacing is negligible. The calculated binding energy is 3.02 eV per supercell for the bilayer Z_6-GNR, higher than 2.53 eV for the bilayer Z_7-GNR, and 2.23 eV for the bilayer Z_5-GNR but smaller than 3.21 eV for the bilayer Z_8-GNR. This is well reflected in the GNR deformation induced by adsorption and the Si-C bond lengths formed between the bottom layer and the substrate: 1.96 ~ 1.98 Å for Z_6-GNR, 1.98 ~ 2.02 Å for the Z_7-GNR, and 1.99 ~ 2.00 Å for the Z_5-GNR.

We calculate the local density of states (DOS) to reveal the change in electronic property at each ribbon layer. A freestanding single-layer Z-GNR shows a sharp DOS peak at the Fermi level due to the localized edge states as show in Fig. 2(a), which leads to spontaneous magnetization with the spin states antiparallel on carbon atoms of different sublattices [A and B in Fig. 1(a)].[22,29] The sharp DOS peak is absent around the Fermi level for the bottom Z_7-GNR in comparison with that of the freestanding counterpart; whereas the localized edge states is regained in the top GNR layer, as indicated by the high DOS at the Fermi level shown in Fig. 2(a). As the high localized DOS at the Fermi level is indicative of a magnetic ground state,[29] an adsorbed bilayer Z-GNR therefore shows spontaneous magnetization at the top GNR layer, while the bottom GNR layer acts as a nonmagnetic buffer layer. This is further evidenced by the distributed magnetization density in the adsorbed bilayer Z_7-GNR shown in Fig. 2(d), where the magnetic orderings are highly concentrated on the top GNR layer and have similar character to that of a freestanding single-layer Z-GNR.

It is interesting to explore why the spin ordering is absent in the bottom layer and retained in the top layer. As the bottom layer covalently bonds to the substrate and only weakly couples to the top layer, the nonmagnetic ground state of the bottom GNR layer is attributed to the formation of equal sp^3-type bonds at its two edges. We take the adsorbed single-layer Z_7-GNR as an example to illustrate this point. Four configurations are considered by symmetrically presetting the sp^3-type bonds from zero to three at each ribbon edge. This is done by selectively removing the terminated hydrogen atoms at the edges of the adsorbed single-layer GNR. We focus our attention on the local partial density of states (LPDOS) of the $2p$ state of the remaining sp^2 edge carbons. Figure 2(b) shows the variation in the LPDOS with the number of the sp^3-type bonds along the ribbon edge. When the sp^3 carbon is absent at ribbon edges as illustrated in the inset of Fig. 2(b), the carbon $2p$ states are strongly localized around the Fermi level, thus leading to Fermi-level instability and a magnetic ground state in the system. However, when sp^3 carbons are inserted into the ribbon edges, a gap is opened around the Fermi level and quickly widened with increasing number of sp^3 carbon bonds. The gap widening reflects a quantum-confinement effect because increasing the sp^3 carbon atoms results in a decrease in regions for the electronic states of sp^2 carbon. The confined sp^2 electronic states show weak spin-exchange interaction and the magnetic ordering at the bottom layer is thus quenched. As the active edge states in the bottom layer have joined in forming the covalent bonding with substrate, the top GNR placed on the bottom layer has a very small binding energy, about 0.021 eV/atom for the Z_7-GNR and 0.020 eV/atom for the Z_6-GNR. This is in stark contrast with the freestanding bilayer Z-GNRs, where the interlayer binding energy is up to 0.05 eV/atom for the bilayer Z_6- and Z_7-GNRs. The reduced interaction from the bottom layer of the adsorbed bilayer makes the magnetic ordering on the top layer survived.

Figures 3(a) and 3(b) present the corresponding spin-polarized band structures of the bilayer Z_6- and Z_7-GNRs adsorbed on the substrate, respectively. The ribbon edge is along the Γ-J direction. Around the Fermi level, the bands in red solid lines are contributed by the top GNR layer and all other bands in dot lines are contributed by the bottom layer and the substrate. If we remove the bands contributed by the top GNR layers from Figs. 3(a) and 3(b), the remaining band structures are reminiscent of the band structures of single-layer Z-GNRs adsorbed on the substrate. It is seen that the bottom layer plus the substrate is semiconducting for the case of Z_6-GNR but metallic for the case of Z_7-GNR, consistent with our previous study of single Z-GNRs on the substrate.[24] On the other hand, the top layer GNR shows a band gap of about 0.21 eV in the case of Z_6-GNR and 0.23 eV in the case of Z_7-GNR, lower than that of 0.33 eV of a freestanding single-layer Z_6- and Z_7-GNRs. In addition, a slight breaking of spin degeneracy is observed for both the top ribbon layers due to asymmetrical interaction of two

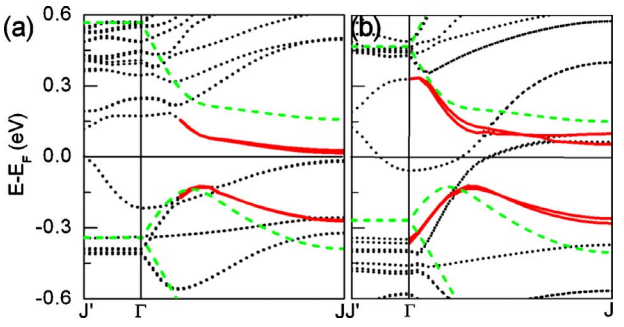

FIG. 3. (Color online) Spin-polarized electronic structures for the ground state of the bilayer (a) Z_6- and (b) Z_7-GNRs adsorbed on the substrates, with the bands of top GNR layer around Fermi level E_F in red (dark) solid lines. The green (light gray) dash lines denote the spin-polarized band structure of the freestanding single-layer Z-GNRs.

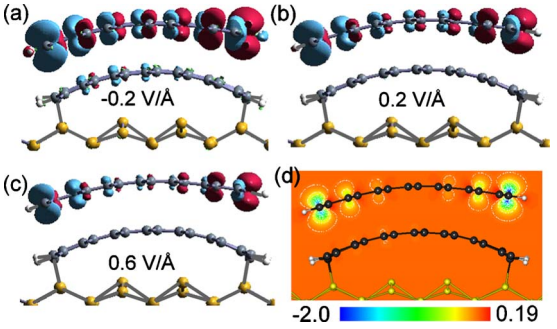

FIG. 4. (Color online) Isosurface plots (0.15 e/Å^3) of magnetization densities (the charge difference between up-spin and down-spin states) for the ground state of the adsorbed bilayer Z_7-GNR on Si(001) under vertical bias voltages of (a) −0.2, (b) 0.2, and (c) 0.6 V/Å. (d) Magnetization density redistribution driven by a positive electric field of 0.2 V/Å, which is calculated by the difference between the magnetization densities at bias voltages of 0.2 and 0.0 V/Å.

edges with the bottom layer. The magnetic moment per edge carbon atom is reduced to $0.19\mu_B$ at the top Z_6-GNR layer and $0.20\mu_B$ at the top Z_7-GNR layer from the pristine value of $0.24\mu_B$ in their freestanding counterparts. Such reduction in the gap and edge magnetization is attributed to the spontaneous charge transfer from the bottom GNR layer to the top layer (see Fig. 7), as a result of lower electrostatic potential at the bottom GNR layer induced by bonding with the substrate. This is in contrast to the freestanding bilayer Z-GNR, where the electrons on both layers transfer to the interlayer space and weak chemical bonds are formed between the ribbon edges of the bilayer (not shown).

B. Magnetic properties in adsorbed bilayer GNR systems under bias voltages

As the edge magnetization can be significantly changed by the charge transfer from the bottom layer, we apply a vertical bias voltage to the adsorbed bilayer systems to tune the interlayer charge transfer, which in turn modulate the edge magnetization of the top GNR layer. We define the positive direction of bias voltage along the normal of the substrate. The magnetization densities for the adsorbed bilayer Z_7-GNR under the bias voltages of −0.2, 0.2, and 0.6 V/Å are shown in Figs. 4(a)–4(c), respectively. It is shown that the magnetization magnitudes on all the carbon atoms of different sublattices decrease with increasing electric field (only for *n*-doped top layer as will be discussed later). The change in magnetization magnitude is most significant at the ribbon edge and exponentially decreases when extending into the ribbon interior, as evidenced by the magnetization density difference at an electric field of 0.2 V/Å illustrated in Fig. 4(d). However, the character of magnetic ordering does not change with the applied bias voltage. In the top ribbon layer, the configuration with opposite spin orientation between ferromagnetically ordered edge states at each edge is still favored as the ground state under different bias voltages. Without the bias voltage, the total energy difference between spin-unpolarized and spin-polarized edge states is 72 meV per supercell (the top Z_7-GNR layer totally contains 48 atoms per supercell), and the antiferromagnetic coupling between two edges of the top Z_7-GNR layer is 12 meV per supercell more favorable than the ferromagnetic coupling. The two values are increased to 107 and 18 meV at a field of −0.2 V/Å but reduced to 36 and 7 meV per supercell at a field of 0.6 V/Å. These results are found to be robust to changing ribbon width. Due to the same character of magnetic ordering as in freestanding Z-GNRs, applying a transverse electric field is possible to convert the top GNR layer into a half-metal[25] and the critical field for achieving the half-metallic state is tunable by the bias voltage.

C. Width dependence of ME effect in adsorbed bilayer GNR systems under bias voltages

Size effect is always an important topic in the research of nanomaterials. It is therefore necessary to investigate the width effect on the ME coupling in the adsorbed bilayer GNR systems. We first calculate the amount of charge transfer from the bottom layer to the top layer for the adsorbed Z_5- to Z_8-GNR bilayer systems as a function of bias voltage as shown in Fig. 5(a). Here, one should note that the electron amount is calculated by using the Bader analysis[30] and the relative change in charge amount is more meaningful than the absolute value. The electrons transferred to the top GNR layer linearly increases with the bias voltage, giving rise to an *n*-to-*p*-type transition in the top GNR layer for all the studied ribbons. However, the transition occurs at different bias voltages: around −0.3 V/Å for the top Z_7-GNR layer and 0.41 V/Å for the top Z_6-GNR. Figure 5(b) presents the magnetic moment per edge carbon atom of A sublattice in the top layer as a function of the bias voltage for the four adsorbed bilayer systems. All the GNRs are found to show carrier-tunable ME effect, namely, the edge moment decreases linearly with increasing bias field in the *n*-doped region but increases linearly in the *p*-doped region. In the linear section, the induced edge magnetization (magnetic moment per unit area) ΔM behaves as $\mu_0 \Delta M = \alpha_S E$, where α_S denotes the surface ME coefficient[17,31] of the top layer. From a linear fit to the calculated data, the ME coefficients

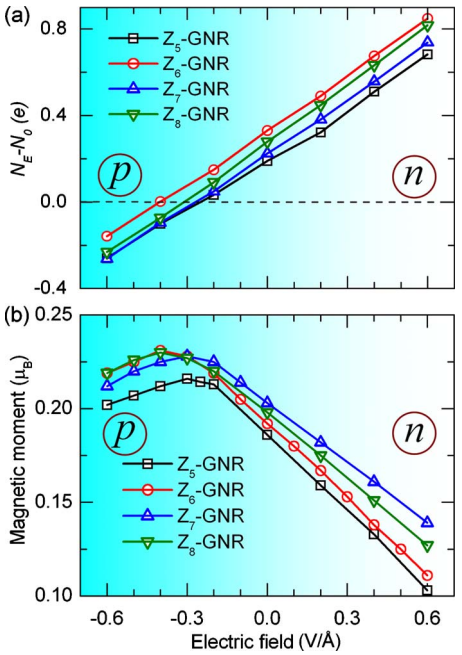

FIG. 5. (Color online) Amount of charge transferred to the top GNR layer as a function of bias voltage for different Z-GNRs. N_E and N_0 present the total number of electrons in the top GNR layer under bias voltage and those in a freestanding single-layer Z-GNR, respectively. (b) Magnetic moment per edge carbon atom at the left ribbon edge of the top GNR layer of different bilayers on the silicon substrate as a function of the applied bias voltage.

(10^{-12} G cm^2/V) of the top Z_5-, Z_6-, Z_7-, and Z_8-GNR layers are calculated to be −0.65, −0.66, −0.53, and −0.58 in the *n*-doped region, and 0.23, 0.29, 0.25, and 0.29 in the *p*-doped region, respectively. It is clear that the ME coefficient oscillates with increasing ribbon width, featuring a notable width effect. As the *p*-doped top layer requires a very high field strength, the ME modulation in *n*-doped region would be more practical for application. We hence will mainly discuss the ME coefficients in the *n*-doped region below.

To better understand this intriguing phenomenon, we explore the underlying mechanism for the distinct width dependence of the ME effect from two perspectives. First, we calculate the change in edge magnetization induced by direct charge injection in freestanding single-layer Z-GNRs, with a uniform positive jellium countercharge, and then convert the injected charge into equivalent electric field according to the linear relationship shown in Fig. 5(a) between extra charge carrier on the top Z_7-GNR layer and applied electric field. The equivalent ME coefficient for a freestanding single-layer Z-GNR is found to decrease with increasing ribbon width. The equivalent coefficients are calculated to be −0.68, −0.67, and −0.64 in the *n*-doped region, and 0.48, 0.36, and 0.28 in *p*-doped region for the single-layer Z_5-, Z_6-, and Z_7-GNRs, respectively. The change in ME coefficient with ribbon width can be understood by plotting their band structures as shown in Fig. 6(a). It is found that the dispersion of the highest valence band increases with increasing ribbon width, leading to delocalization of the hole edge states, while that of the lowest conduction band shows inconspicuous change with ribbon width. Therefore, when extra holes enter the Z-GNRs,

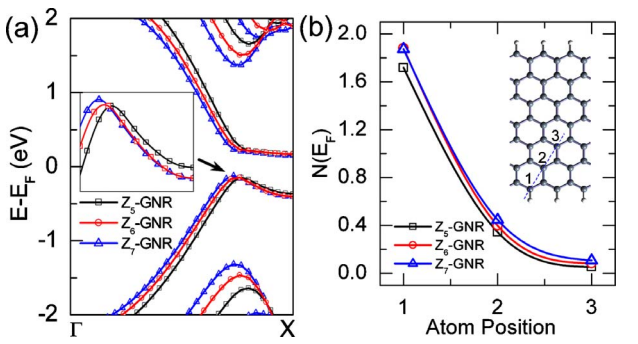

FIG. 6. (Color online) (a) Spin-polarized band structures of the freestanding single-layer Z_5-, Z_6-, and Z_7-GNRs. (b) Spin-unpolarized local DOS at the Fermi level at the carbon atoms 1, 2, and 3 along the dot line shown in the inset for freestanding Z-GNRs, which reflect the decay length of the edge states.

more localized hole edge states in narrower ribbons leads to larger ME coefficient in the *p*-doped region. On the other hand, the equivalent ME coefficient in the *n*-doped regions decreases with increasing ribbon width due to the increased decay length of the localized edge states with increasing ribbon width, as shown in Fig. 6(b). Increasing decay length makes the edge states distribute on more atoms in the GNRs. So the injected electrons occupying the edge states will distribute on more carbon atoms in wider GNRs, which leads to smaller change in edge magnetization and thus smaller ME coefficient, although this effect is not as pronounced as the delocalization of the hole edge states. These results suggest that the ME effect in Z-GNRs has an intrinsic width dependence. However, the intrinsic width dependence will disappear if the ribbon width is significantly larger than the decay length of the spin-polarized edge states.[32]

Second, the interaction from the bottom layer also considerably influences the ME effect of the top GNR layer, which is dependent on the covalent binding strength between the bottom layer and the substrate. Stronger binding strength leads to weaker coupling of the top layer with the bottom layer, and the screening effect of the bias voltage will be enhanced across the bilayer. As a result, the bias-driven interlayer charge transfer is different for different adsorbed bilayer Z-GNRs. This is reflected by the different slopes of transferred charge versus bias voltage shown in Fig. 5(a). The hierarchy of slope value is given by Z_8-GNR $>Z_6$-GNR$>Z_7$-GNR$>Z_5$-GNR. On the other hand, the interaction from the bottom layer also affects the redistribution of the transferred charge in the top ribbon layer. To clarify this issue, we plot the interlayer charge redistribution induced by placing the top GNR layer over the bottom layer under different bias voltages for the bilayer Z_6- and Z_7-GNRs, as shown in Figs. 7(a) and 7(b), respectively. Without the bias voltage, the charge accumulation is highly concentrated at the two edges of the top Z_6-GNR but distributes more delocalized across the Z_7-GNR. Especially, part of the accumulated charge is distributed away from the ribbon planar in the adsorbed bilayer Z_7-GNR. This difference in charge redistribution is basically maintained in the presence of the bias voltage. As a result, a considerable amount of transferred charge cannot affect the filling and thus the ex-

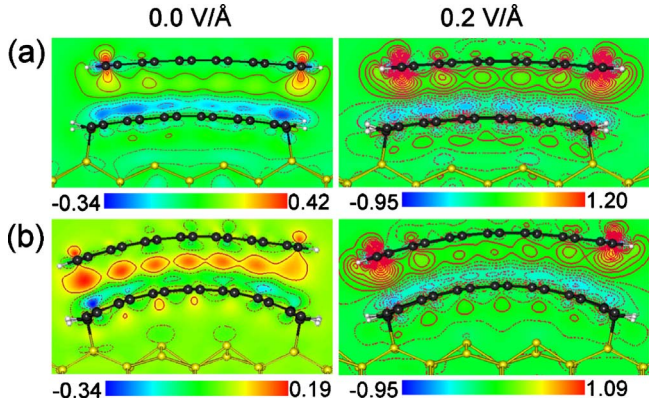

FIG. 7. (Color online) Charge redistributions induced by adsorption of the top (a) Z_6- and (b) Z_7-GNR layers under bias voltages of 0.0 and 0.2 V/Å. Red (solid lines) and blue (dot lines) colors indicate charge accumulation and depletion regions, respectively. The contour spacing is uniformly set to be 80×10^{-3} e/Å^3.

change splitting of the edge states of the Z_7-GNR since they are accumulated away from the ribbon planar, leading to a smaller variation in the edge magnetization. This effect of the interaction from bottom layer changes the ME coefficient in the *n*-doped region from freestanding *equivalent* value of −0.64 to −0.53 for the top Z_7-GNR. The binding strength between the bottom layer and the substrate mainly depends on the lateral mismatch strain between them, which is smaller for the Z_6-GNR than that for the Z_7-GNR. Such mismatch strain can be reduced with further increasing the width of a wider bilayer GNR. Based on above analysis, we conclude that the interplay between the intrinsic ribbon-width effect of the edge states and the binding-dependent charge transfer from the bottom layer leads to the distinct oscillation of ME coefficient with ribbon width. Since both the intrinsic width effect and the interaction from the bottom layer trend to be constant with increasing ribbon width, it is expected to yield a stable ME modulation in the adsorbed bilayer Z-GNRs within a certain range of ribbon width. Although these analyses shed light on the ribbon-width-dependent behavior of the ME effect on Z-GNRs, a full understanding of this interesting property still requires additional work, especially a systematic study of wider Z-GNRs which are beyond our current computing capability. For bilayer Z-GNRs of experimental size, covalent Si-C bonds also form at the ribbon interior other than the ribbon edges, which may give rise to a different width-dependent effect. Nevertheless it has been shown that the ME effect remains robust against variations in material and physical configurations over a large range.[18]

D. Effect of ribbon length on the magnetic modulation

We also considered the finite-sized GNRs. As revealed in previous study,[33] a finite-sized Z-GNR does not show magnetic edge states until its length reaches 11.8 Å (i.e., four primitive cells). So calculating the ME coupling in the finite-sized GNR on the silicon substrate is beyond our computational capability. However, as the ME coupling is induced by the bias-driven charge transfer from the substrate, we can simulate the ME modulation in freestanding finite-sized Z-GNRs by charge injection, with a uniform jellium model. We find that similar ME modulation still exists in these finite-sized Z-GNRs, if the injected charge is converted into electric field strength (Fig. 8). Moreover, we do not observe remarkable length effect in the magnetic modulation, suggesting that the magnetic modulation also holds for the finite-sized GNRs. This is meaningful considering that current device dimension continues to shrink. Further study is necessary to clarify the length effect involving the substrate under bias voltage.

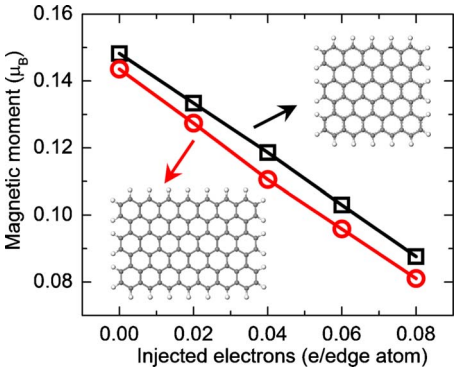

FIG. 8. (Color online) Magnetic moment per edge carbon atom of two finite-sized Z_6-GNRs consisting of five and seven hexagons along the zigzag edge as a function of injected electrons per edge atom.

E. Bias-induced modulation in electronic properties of the adsorbed bilayer Z-GNRs

We also consider another key parameter for electronic device applications: the band gap of the top GNR layer. In the aforementioned discussion, the bandgap of the top GNR layer at zero-bias voltage exhibits a large reduction compared to that of the corresponding freestanding single-layer Z-GNR due to intrinsic interlayer charge transfer. As the bias voltage can tune the interlayer charge transfer, the band gap of the top GNR layer should also vary concomitantly with the ME coupling. Figure 9 presents the band gap of the top Z_5-, Z_6-, and Z_7-GNR layers as a function of the applied bias voltage. It is shown that the band gap decreases with increasing bias voltage in the *n*-doped region but increases in the *p*-doped region, demonstrating a similar character to the change in edge magnetization in Fig. 5(b). The ratio of bandgap variation with respect to the bias voltage is largest for the Z_6-GNR and smallest for the Z_7-GNR, also showing the same variation feature in ME coefficient with ribbon width. This is because the band gap is due to the spin splitting of the localized magnetic edge states that is proportional to the edge magnetization. The underlying mechanism for the gap variation can be further understood by examining the DOS of the localized edge states at different bias voltages. In the spin-unpolarized case, the Z-GNR is metallic with a sharp DOS peak just located at the Fermi level. Local electron-electron interaction will make the localized edge states polarized and split, lowering the system energy and forming a

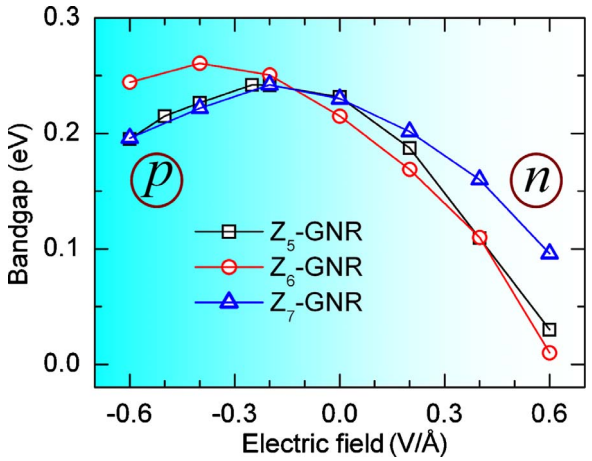

FIG. 9. (Color online) Band gap of the top Z_5-, Z_6-, and Z_7-GNR layers in the adsorbed bilayer systems as a function of the bias voltage.

band gap around the Fermi level. The splitting of the localized edge states significantly depends on the DOS value at the Fermi level,[34] which can be modulated by the bias-induced interlayer charge transfer, see Fig. 10(a). Figure 10(b) illustrates the evolution of the localized edge states and their spin splitting under different bias voltages. It is clear that the bias-induced charge transfer controlling electron population of the localized edge states dominates the band-gap modulation in the top layer. In contrast, the field-induced variation in atomic structures of the system is much smaller, the effect of which on the electronic properties is negligible as examined by our test calculations.

An important merit of the gap modulation is that the top GNR layers can switch to metals under bias voltage, resulting in a semiconductor-to-metal transition. Figure 11 exhibits the spin-polarized band structures for the adsorbed bilayer Z_6- and Z_7-GNRs under different bias voltages. Without the applied electric field, both the top Z_6- and Z_7-GNR layers are semiconductors as there are no involved bands crossing the Fermi level. Under the bias voltage of 0.2 V/Å, the highest conduction bands of the top GNR layer start to cut the Fermi

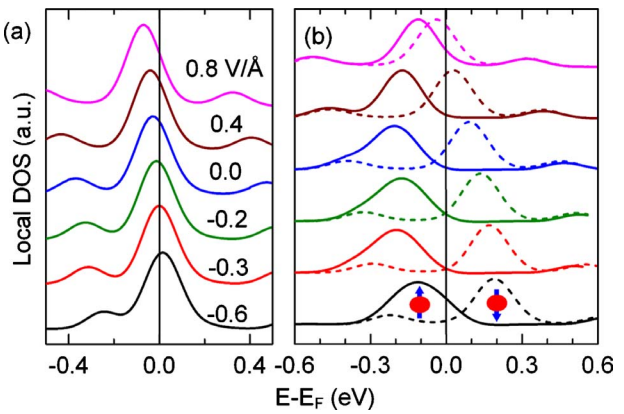

FIG. 10. (Color online) (a) Average local spin-unpolarized DOS of the left edge carbon atom in the top Z_7-GNR layer under bias voltages from −0.6 to 0.8 V/Å. (b) Corresponding local spin-up (solid lines) and spin-down (dash lines) DOS.

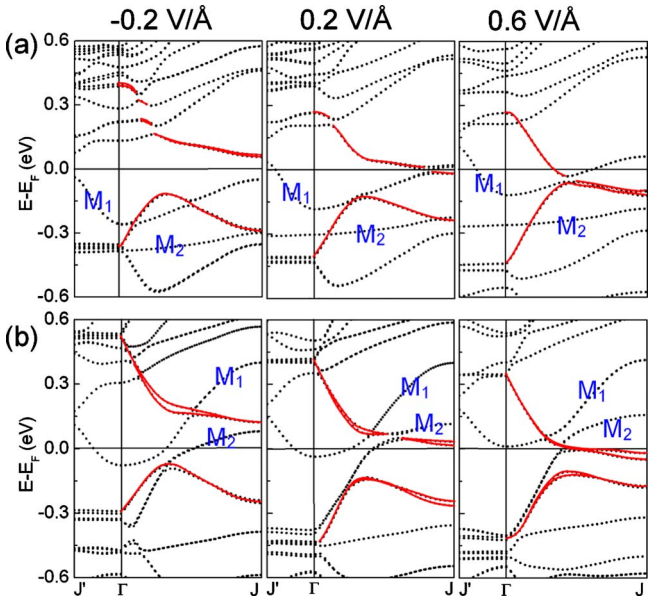

FIG. 11. (Color online) Spin-polarized band structures for the ground state of the adsorbed bilayer (a) Z_6- and (b) Z_7-GNRs on the substrate under different bias voltages. The bands of top GNR layer around the Fermi level E_F are highlighted in red solid lines.

level for both the ribbons, rendering them being semimetallic. With further increasing bias voltage, the highest conduction bands will cross the Fermi level and both the top ribbon layers become metallic, as in the case of 0.6 V/Å, for example. Such a semiconductor-to-metal transition is due to the increase in bias-induced carrier accumulation in the top layer which makes the lowest conduction band partially occupied. On the other hand, the lowest valence band of the top GNR layer can also be moved closer to the Fermi level by applying a negative bias voltage. However, it needs much higher negative bias voltage to make the lowest valence band across the Fermi level, which, for example, is up to −0.7 V/Å for the top Z_6-GNR, due to the large energy distance from the valence-band maximum to the Fermi level. As the substrate thickness of our calculated model is thin, the bias-driven amount of charge transfer to the top layer is somewhat small. Increasing the substrate thickness would enhance the electric field screening to increase the charge transfer, as has been demonstrated in our previous work for ME effect.[18] Therefore, with experimental substrates of several hundreds of nanometers thick, the band gap of the top layer will be sensitively modulated by the bias voltage and the semiconductor-to-metal transition would occur at much lower field strength, thereby making it feasible for practical device applications. Also, we are aware of that the local-density-approximation calculations underestimate the band gaps of graphene ribbons. However, the semiconductor-metal transition in the top GNR layer is due to the bias-driven charge transfer occupying the empty conduction-band states, and it should be robust to quasiparticle self-energy corrections, which only raise the energy levels of conduction-band bottom. Similar charge-transfer-induced metallization have been observed experimentally in epitaxial graphene on SiC.[35]

Another interesting result is that the band gap of the whole adsorbed bilayer Z_6-GNR system is also tunable by

bias voltage. The system band gap increases from 0.02 eV at 0.0 V/Å to 0.11 eV at −0.2 V/Å while becoming completely closed in the region of positive bias voltage, as shown in Fig. 11(a). In contrast, the whole adsorbed bilayer Z_7-GNR system remains metallic regardless of the field strength and direction. This difference results from different hybridization between the bottom layer and substrate. In the case of Z_6-GNR, the valence states of the bottom layer interact with the valence-band states of the substrate, resulting in two mixed states, M_1 and M_2, below the Fermi level, see Figs. 3(a) and 11(a). Under applied bias voltages, the M_1 state shifts up or downward with respect to the Fermi level, thus changing the system band gap and leading to the metal-to-semiconductor transition once the M_1 state crosses the Fermi level. In contrary, in the case of the Z_7-GNR, the valence states of the bottom layer interact with the conduction-band states of the substrate, resulting in two mixed states M_1 and M_2 crossing the Fermi level [Fig. 11(b)] and making the system always being metallic even under bias voltages. Stronger binding of the bottom layer with the substrate in the adsorbed bilayer Z_6-GNR is crucial for the appearance of semiconducting properties in the whole system.[24]

IV. CONCLUSIONS

In summary, we have performed a comprehensive first-principles study on bias-voltage-induced modulation of magnetic and electronic properties of bilayer Z-GNRs on Si(001) substrate. When a nonmagnetic bilayer Z-GNR is placed on the substrate, the bottom layer remains nonmagnetic while the top layer shows magnetic ordering similar to that of a freestanding Z-GNR. Applied bias voltage can tune the magnitude of edge magnetization on the top layer without changing the character of the magnetic ordering. Bias-voltage-induced ME coupling in the system is found to be width dependent and the calculated ME coefficient oscillates with increasing ribbon width and is expected to converge in wider bilayer GNRs. The underlying mechanism for the width dependence is elucidated in terms of the GNR-substrate interaction and the inherent width-dependent effect in freestanding single-layer Z-GNRs. Meanwhile, the band gap of the top GNR layer shows similar modulation to edge magnetization by bias voltage. Interestingly, the top GNR layers can switch to metallic states under bias voltages above a critical strength due to increased carrier accumulation in the top GNR layer occupying the subbands. Moreover, a bias-voltage-induced semiconductor-to-metal transition is also observed in the bilayer adsorption system when the bottom GNR layer is semiconducting. These results demonstrate a rich variety of electronic and magnetic properties of bilayer GNRs on Si substrates that can be effectively tuned by applied bias voltages, which may pave a path toward graphene-based devices on silicon chips for both nanoelectronics and spintronics applications.[36]

ACKNOWLEDGMENTS

W.G. was supported by the 973 Program (Grant No. 2007CB936204), NSF (Grant No. 10732040) and Jiangsu Province NSF (Grant No. BK2008042). C.F.C. was supported by the U.S. Department of Energy under Cooperative Agreement No. DE-FC52-06NA26274. X.C.Z. was supported by grants from NSF (Grants No. CHE-0427746 and No. DMR-0820521) and the Nebraska Research Initiative, and by the University of Nebraska Holland Computing Center. Z.Z. was also supported by the Jiangsu Province Scientific Research Innovation Project for Graduate Students (Contract No. CX07B-064z).

*wlguo@nuaa.edu.cn

[1] E. B. Myers, D. C. Ralph, J. A. Katine, R. N. Louie, and R. A. Buhrman, Science **285**, 867 (1999).
[2] J. Rondinelli, M. M. Stengel, and N. A. Spaldin, Nat. Nanotechnol. **3**, 46 (2008).
[3] W. Eerenstein, N. D. Mathur, and J. F. Scott, Nature (London) **442**, 759 (2006).
[4] M. Fiebig, J. Phys. D **38**, R123 (2005).
[5] I. Dzyaloshinskii, Sov. Phys. JETP **10**, 628629 (1960).
[6] D. Astrov, Sov. Phys. JETP **11**, 708709 (1960).
[7] G. Srinivasan, E. T. Rasmussen, J. Gallegos, R. Srinivasan, Y. I. Bokhan, and V. M. Laletin, Phys. Rev. B **64**, 214408 (2001).
[8] C. Binek and B. Doudin, J. Phys.: Condens. Matter **17**, L39 (2005).
[9] N. A. Spaldin and M. Fiebig, Science **309**, 391 (2005).
[10] R. Ramesh and N. A. Spaldin, Nature Mater. **6**, 21 (2007).
[11] T. Zhao, A. Scholl, F. Zavaliche, K. Lee, and M. Barry, Nat. Mater. **5**, 823 (2006).
[12] D. Chiba, M. Sawicki, Y. Nishitani, Y. Nakatani, F. Matsukura, and H. Ohno, Nature (London) **455**, 515 (2008).
[13] M. Weisheit, S. Fahler, A. Marty, Y. Souche, C. Poinsignon, and D. Givord, Science **315**, 349 (2007).
[14] D. Chiba, M. Yamanouchi, F. Matsukura, and H. Ohno, Science **301**, 943 (2003).
[15] Y. H. Chu, L. W. Martin, M. B. Holcomb, M. Gajek, S. Han, Q. He, N. Balke, C. Yang, D. Lee, W. Hu, Q. Zhan, P. Yang, A. F. Rodriguez, A. Scholl, S. X. Wang, and R. Ramesh, Nature Mater. **7**, 478 (2008).
[16] C. G. Duan, S. S. Jaswal, and E. Y. Tsymbal, Phys. Rev. Lett. **97**, 047201 (2006).
[17] C. G. Duan, J. P. Velev, R. F. Sabirianov, Z. Zhu, J. Chu, S. S. Jaswal, and E. Y. Tsymbal, Phys. Rev. Lett. **101**, 137201 (2008).
[18] Z. H. Zhang, C. F. Chen, and W. L. Guo, Phys. Rev. Lett. **103**, 187204 (2009).
[19] H. Lee, N. Park, Y. W. Son, S. Han, and J. Yu, Chem. Phys. Lett. **398**, 207 (2004).
[20] M. P. Lima, A. Fazzio, and A. J. R. da Silva, Phys. Rev. B **79**, 153401 (2009).
[21] Y. W. Son, M. L. Cohen, and S. G. Louie, Phys. Rev. Lett. **97**, 216803 (2006).
[22] J. Jiang, W. Lu, and J. Bernholc, Phys. Rev. Lett. **101**, 246803 (2008).

[23] L. Yang, M. L. Cohen, and S. G. Louie, Phys. Rev. Lett. **101**, 186401 (2008).
[24] Z. H. Zhang and W. L. Guo, Appl. Phys. Lett. **95**, 023107 (2009).
[25] Y. W. Son, M. L. Cohen, and S. G. Louie, Nature (London) **444**, 347 (2006).
[26] G. Kresse and J. Hafner, Phys. Rev. B **49**, 14251 (1994).
[27] G. Kresse and J. Furthmuller, Phys. Rev. B **54**, 11169 (1996).
[28] J. Neugebauer and M. Scheffler, Phys. Rev. B **46**, 16067 (1992).
[29] M. Fujita, K. Wakabayashi, K. Nakada, and K. Kusakabe, J. Phys. Soc. Jpn. **65**, 1920 (1996).
[30] G. Henkelman, A. Arnaldsson, and H. Jonsson, Comput. Mater. Sci. **36**, 354 (2006).
[31] C. G. Duan, C. W. Nan, S. S. Jaswal, and E. Y. Tsymbal, Phys. Rev. B **79**, 140403(R) (2009).
[32] H. Lee, Y. W. Son, N. Park, S. Han, and J. Yu, Phys. Rev. B **72**, 174431 (2005).
[33] D. Jiang, B. G. Sumpter, and S. Dai, J. Chem. Phys. **127**, 124703 (2007).
[34] D. M. Edwards and M. I. Katsnelson, J. Phys.: Condens. Matter **18**, 7209 (2006).
[35] S. Y. Zhou, G. H. Gweon, and A. V. Fedorov, Nature Mater. **6**, 770 (2007).
[36] S. P. Dash, S. Sharma, R. S. Patel, M. P. de Jong, and R. Jansen, Nature (London) **462**, 491 (2009).